Corrosion inhibition of sulphate-reducing bacterial by Ag/Cu bimetallic nanoparticles synthesised from ginger extract

Link to publication record in Ulster University Research Portal

Document Version
Author Accepted version

Journal Pre-proof

Corrosion inhibition of sulphate-reducing bacterial by Ag/Cu bimetallic nanoparticles synthesised from ginger extract

Yujie Hu, Qing Feng, Hao Zeng, Ibrahim M. Banat, Yinfang Si, Peixiu Huang, Xiaonan Li, Shanshan Sun, Hao Dong, Yuehui She, Fan Zhang

CRediT author statement

Yujie Hu: Methodology, Validation, Data Curation, Writing-Original Draft, Writing-Review &Editing. **Qing Feng, Xiaonan Li:** Project administration. **Hao Zeng:** Formal analysis. **Ibrahim M. Banat:** Supervision. **Yinfang Si , Peixiu Huang:** Visualization. **Shanshan Sun, Hao Dong:** lnvestigation. **Yuehui She:** Conceptualization, Funding acquisition. **Fan Zhang:** Resources.
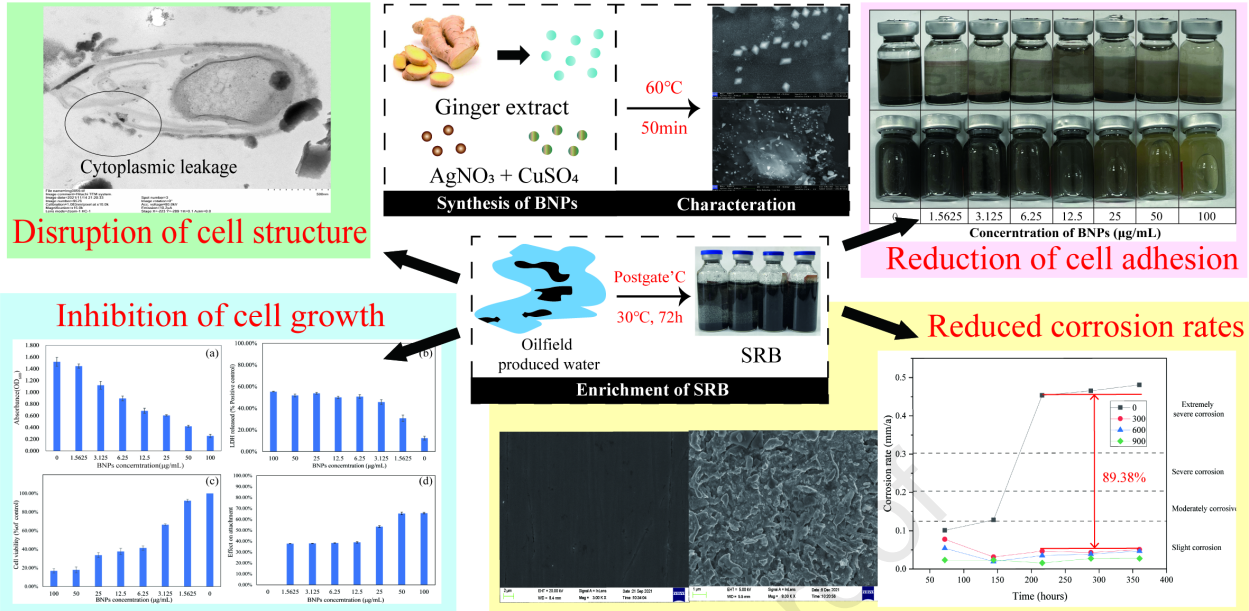
Corrosion inhibition of sulphate-reducing bacterial by Ag/Cu bimetallic nanoparticles synthesised from ginger extract

Yujie Hu[a, b], Qing Feng[c], Hao Zeng[a, b], Ibrahim M. Banat[d], Yinfang Si[a, b], Peixiu Huang[a, b], Xiaonan Li[c], Shanshan Sun[a, b], Hao Dong[e], Yuehui She*[a, b], Fan Zhang*[f]

[a.] College of Petroleum Engineering, Yangtze University, Wuhan, 430010, China;

[b.] Hubei Key Laboratory of Drilling and Production Engineering for Oil and Gas, Wuhan, 430010, China;

c. Oilfield Production Optimization Institution of China Offshore Oilfield Services Limited, Tianjin, 300459, China;

[d.] Faculty of Life and Health Sciences, University of Ulster, Coleraine BT52 1SA, UK

[e.] College of Chemical and Environmental Engineering, Yangtze University, Jingzhou, 434023, China;

[f.] The Key Laboratory of Marine Reservoir Evolution and Hydrocarbon Accumulation Mechanism, Ministry of Education, College of Energy Resources, China University of Geosciences (Beijing), Beijing 100083, China.

* Corresponding author:

Yuehui She (sheyuehui@163.com); Fan Zhang (fanzhang@cugb.edu.com).

Graphic Abstract:
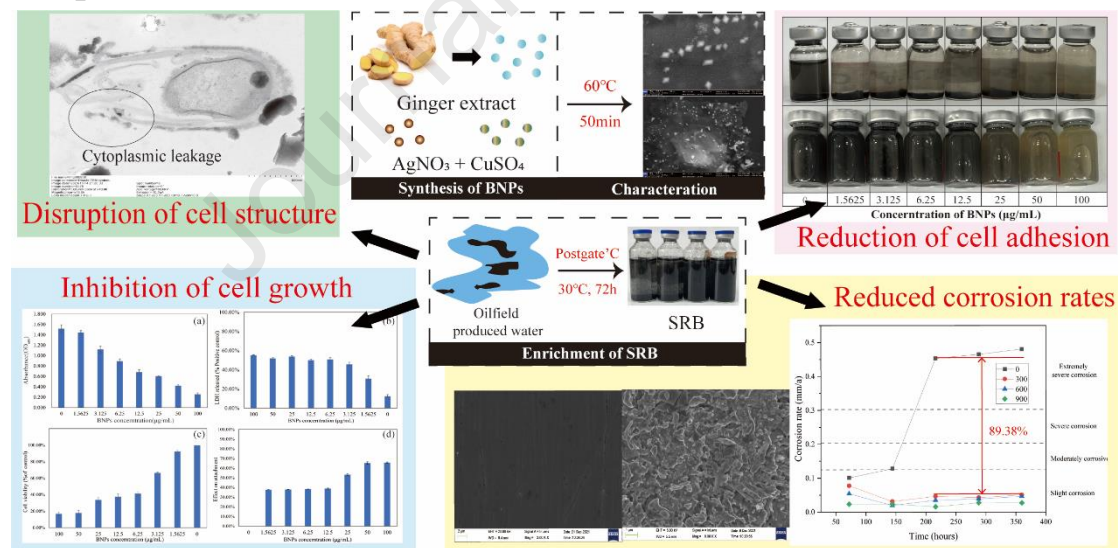
Highlights:

1. Ginger extract can be used for the synthesis of bimetallic nanoparticles (BNPs).

2. BNPs can reduce the adhesion of SRB on carbon steel surface.

3. SRB cells ruptured by BNPs can slow down the rate of weight loss of carbon steel.

4. This paper provides a promising option for reducing the drug resistance of SRBs.

Abstract: The growth of sulphate-reducing bacteria (SRB) in oilfield produced water and resistance to antibiotics has become an important issue for safe and clean production. Bimetallic nanomaterials with antibacterial effects are a potential candidate to confront microbial resistance. Environmentally friendly methods for the synthesis of bimetallic nanomaterials are an important factor to be considered in production. This study proposed a green method to synthesise Ag/Cu bimetallic nanoparticles (BNPs) as novel corrosion inhibitors and biocides using ginger rhizome extracts.The results showed that 6.25 $\mu g \cdot mL^{-1}$ BNPs synthesised from ginger extract could disrupt the integrity of SRB cells and reduce adhesion on the surface of carbon steel over 65%. The corrosion rate of BNPs-treated SRB cultures on carbon steel was verified by weight tests, decreasing from 0.453 $mm \cdot a^{-1}$ to 0.05 $mm \cdot a^{-1}$. The changes of carbon steel surface morphology and SRB cell structure after BNPs treatment were observed in order to illustrate the inhibition mechanism of BNPs. The corrosive inhibitors prepared by this method have potential in inhibiting the corrosion behaviour of SRBs and are expected for applications in oilfield production for pipeline corrosion protection.

Keywords: Ginger extract; Ag/Cu bimetallic nanoparticles; Antibacterial activity; Corrosion Inhibition; Green fabrication

1. Introduction

Sulphate-reducing bacteria (SRB) are distributed widely in soil and water, and their enrichment and growth can produce hydrogen sulphide gasand ferrous sulfide fouling (Khan et al., 2021). Sulphides produced by bacterial metabolism have a significant effect on the acidification of oil reservoirs, causing great potential safety hazards and nearly $875 billion in economic losses to oil fields each year (Bolaji et al., 2019). SRB is the widely studied microbial group in the petroleum industry because it can obtain energy by coupling oxidised organic matter or hydrogen with different sulphate reduction (Procópio, 2022). Biofilm colonisation in oil production facilities is dominated by the SRB group of *Desulfovibrio* sp., which can exacerbate pipeline corrosion and affects oil quality (Nasser et al., 2021). Extracellular polymeric substances (EPS) synthesised after the free cells adhere to the metal surface will allow the aggregation of different microbial species. The persistence and maturation of biofilms drive internal environmental variations that can create anaerobic conditions and a more acidic pH at metal–contact sites (Garcia and Procopio, 2020). It enables the environment to assume a more favourable environment for the survival of corrosive

64 microorganisms and can induce or accelerate metal corrosion through different

65 mechanisms. The presence of sulphate and iron in petroleum and anaerobic

66 environment in deep formations results in the proliferation of typical anaerobic

67 microbial members in microbiologically influenced corrosion. Biofilms resistant to

68 common bacteriostatic agents are then formed (Rabus et al., 2016). In addition,

69 chemical fungicides generally adopted in the oilfield in the past were glutaraldehyde,

70 dibromo-nitropropionamide (DBNPA), phosphonium tetra (hydroxymethyl) sulphate

71 (THPS) and alkyl dimethyl benzyl ammonium chloride (Pereira et al., 2021). Increasing

72 drug resistance was exhibited by SRB due to their instability in the extreme

73 environmental conditions of the oilfield (Parmar et al., 2022).

74   Nanotechnology is effective in controlling microorganisms that are resistant to

75 drugs caused by biofilms (Huh and Kwon, 2011). Biofilms are the associations of

76 microbial cell populations that can adhere to living and non-living surfaces with the

77 assistance of extracellular polymeric substances and glycocalyxes (Hayat et al., 2018).

78 Nanoparticles (NPs) can inhibit biofilm formation by inhibiting bacterial growth

79 through exopolysaccharide penetration of the biofilm matrix, affecting the quorum

80 sensing gene cascade within the biofilm and thus impeding the intercellular

81 communication mechanism (Arora et al., 2020). The main mechanisms of nanomaterial

82 bactericidal are (1) disturbance of homeostasis through protein binding; (2) cell

83 membrane degradation through electrostatic interactions; (3) reactive oxygen specie

84 (ROS) generation and oxidative stress; (4) disruption of proteins and enzymes (Huh

85 and Kwon, 2011); (5) genotoxicity and signal transduction inhibition; and (6)

86 photocatalytic degradation mechanism (Marslin et al., 2018). These antimicrobial

87 mechanisms allow nanomaterials to exhibit superior capabilities compared with

88 conventional antibiotics. Microorganisms treated with NPs effectively inhibit biofilm

89 formation and activate other related processes, thereby preventing the establishment of

90 drug resistance (Moritz and Geszke-Moritz, 2013). In contrast to conventional

91 antibacterial agents, these nanomaterials can be employed to carry and deliver

92 additional antibacterial drugs, i.e., operate as drug delivery scaffolds while exhibiting

93 antimicrobial activity by themselves. Bimetallic nanoparticles (BNPs) have more

94 potential applications than their monometallic counterparts due to the different catalytic

95 and synergistic properties between the two different metals (Sumbal et al., 2019).

96 Characteristics, such as size, shape, zeta potential and large specific surface area of

97 bimetallic nanomaterials, are conducive to their effective interaction with bacterial cell

98   membrane, resulting in the destruction of the host immune system, the production of
99   reactive oxygen species, protein dysfunction and DNA damage (Basavegowda and
100   Baek, 2021). BNPs exhibit significant performance compared with commonly used
101   antibiotics and other antimicrobial treatments. Pathogens cannot have resistance to
102   them because they inhibit biofilms generation and accelerate other related processes,
103   including altering the osmotic pressure of the membrane and reducing adhesion
104   behaviour (Birk et al., 2021).

105   BNPs mediated by plants are more practical because they do not require such
106   complex procedures as isolation or well-conditioned culture and its maintenance. It is
107   very economical because the production of large quantities of NPs can be directly
108   simplified and the association of toxic substances can be further mitigated (Kaabipour
109   and Hemmati, 2021). Secondary metabolites in plant extracts, such as flavonoids (Jebril
110   et al., 2020), alkaloids (Kamli et al., 2021), terpenoids (Merugu et al., 2021),
111   heterocyclic compounds (Patra et al., 2018), polysaccharides, organic acids (Seetha et
112   al., 2020), proteins and vitamins, have been used as sources of reducing and capping
113   agents in nanosynthesis, which can form stable NPs quickly and safely. The extraction
114   of Oleuropein was found to form an outer film on metal surfaces as a natural metal
115   corrosion inhibitor in a recent study by Deyab et al (2022). This method was used to
116   develop corrosion inhibitors as a cost-effective strategy for corrosion inhibition of
117   carbon steel. Plant extracts are receiving increasing attention from researchers as a low-
118   cost, biodegradable and environmentally friendly agent (Fazal et al., 2022).

119   A plant-based bimetallic nanomaterial has been prepared as a corrosion inhibitor
120   for oilfield production, considering both the use of plant extracts as corrosion inhibitors
121   and nanomaterials with high surface energy catalytic and cytotoxic characteristics. The
122   ginger oleoresin in ginger extract contains benzene rings, hydroxyl groups, carbonyl
123   groups and other polar groups with reducing properties (Babaeekhou and Ghane, 2021).
124   Metal ions can be reduced to zero-valent metals by the reducing substances in them (El-
125   Refai et al., 2018). And the polar groups are adsorbed on the metal surface to form a
126   film that avoids particle aggregation (Saleh et al., 2018). Studies have reported the use
127   of nanomaterials for surface modification of carbon steel to inhibit SRB-influenced
128   corrosion (Cai et al., 2021). Although this method can achieve good corrosion inhibition,
129   replacing most of the pipelines in production would require a huge workload. In this
130   study, Ag/Cu BNPs were synthesised from ginger extract and used to inhibit SRBs in
131   oil pipelines, which provides a new idea for green production in oil fields. This is a

132 rapid and environmentally friendly nano-synthesis method compared to past studies. It

133 also achieved the inhibition of SRB growth using lower concentrations of bacterial

134 inhibitors. It is particularly effective against SRB communities that have developed

135 resistance to chemical inhibitors.

136   In this study, a green method to prepare plant-based corrosion inhibitors for oilfield

137 applications was proposed. The synthesised BNPs were characterised by UV

138 spectrophotometry and scanning electron microscopy. The ginger extracts were

139 analysed to determine active substances in the synthesis process. In addition, the

140 antibacterial mechanism and anti-adhesive activity of Ag/Cu BNPs against SRB

141 affecting corrosion were evaluated. The effectiveness of products in contributing to

142 cleaner production in oil fields was proven.

143

2. Materials and methods

2.1 Materials

146   Fresh ginger was obtained from Yueyang, Hunan, China. Silver nitrate ($AgNO_3$,

147 99.9%) and copper sulphate pentahydrate ($CuSO_4 \cdot 5H_2O$, 99.9%) were purchased from

148 chemical reagent company in Shanghai, China. The SRB samples used for

149 antimicrobial experiments were enriched from oilfield-produced water from a field in

150 central China. Q235 steel was used to study the degree of corrosion. All solutions during

151 the reaction were prepared with deionised water.

2.2 Synthesis of Ag/Cu bimetallic nanoparticles (Ag/Cu BNPs)

2.2.1 Preparation of ginger aqueous extract

154   In brief, 100 g of fresh ginger was washed in distilled water to remove surface soil

155 and sliced into thin slices of 2.0 mm thickness. Ginger extract was prepared in a 50 min

156 water bath with ginger slices completely submerged in 500 mL of deionised water at

157 60°C (López-Ubaldo et al., 2020). The extract was centrifuged (Xiang Yi, H2050R) at

158 6000 rpm and 4°C for 5 min. The plant residues were then removed using ordinary filter

159 paper on a vacuum extraction unit to obtain plant extracts and stored in a 4°C

160 refrigerator for use.

2.2.2 Green synthesis of BNPs

162   Ag/Cu BNPs were synthesised using 5 mL of silver nitrate solution (0.025 mM)

163 and 5 mL of copper sulphate pentahydrate (0.075 mM) solution as precursors. The

164 sample was added to a conical flask containing 40 mL of the ginger extract. The mixture

165 was placed in a water bath at 60°C for 30 min until the colour of the solution changed

166 from light yellow to brownish green, indicating the formation of BNPs (Merugu et al.,

167 2021). The mixture was centrifuged at 10,000 rpm and 4°C for 5 min after standing

168 overnight and then freeze-dried under vacuum.

169 **2.3 Characterization of biosynthesised BNPs**

170 **2.3.1 Particle size determination**

171 After the mixture of extracts and nanoparticles was ultrasonically dispersed, the

172 particle size of the nanoparticles was measured using a laser particle size meter

173 (Bettersize 2600) and the stability of the extract was determined. The formation of

174 Ag/Cu BNPs was determined by UV-Vis spectra obtained in the 200–800 nm by using

175 a Yippu Instrument Manufacturing U-T6 UV spectrophotometer.

176 **2.3.2 Scanning electron microscopy (SEM)**

177 The detailed microstructural observations and particle morphology of BNPs were

178 performed under a high-resolution Zeiss Merlin Compact scanning electron microscope

179 (SEM). The acceleration voltage at 15 kV has an amplification of 40 kX. The sample

180 surface was sprayed with a very thin layer of gold by vapor deposition to ensure good

181 electrical conductivity.

182 **2.3.3 Energy-dispersive X-ray spectroscopy (EDX)**

183 An EDX detector (Oxford Instruments) was connected to the SEM instrument.

184 Energy-dispersive X-ray spectrometry was used to obtain the composition and

185 elemental analysis of Ag/Cu BNPs to determine silver and copper.

186 **2.3.4 Fourier transformed infrared spectroscopy (FTIR)**

187 The chemical composition of ginger extracts and BNPs was analysed at room

188 temperature by using an FTIR spectrometer (Thermo Scientific Nicolet 6700). The

189 ginger extract before and after synthesis was analysed separately to determine the active

190 components in the ginger aqueous extract responsible for the reduction of metal ions.

191 Infrared spectra were recorded by scanning 32 times in the range of 4000–400 cm^{-1}

192 with a resolution of 4 cm^{-1}, and signal peaks were labelled.

193 **2.4 Antibacterial tests**

194 The antimicrobial performance of BNPs was tested on SRB cultures isolated from

195 oilfield-produced water, which generated hydrogen sulphide gas. The mixture was

196 counted by serial dilution to 10^8 CFU·mL^{-1} (0.5 McFarland standardised inoculum) by

197 anaerobic incubation in Postgate'C medium (biochemical reagent company in Qingdao,

198 China) at 30 °C for 14 days. The 96-well plates were incubated in an anaerobic

199 incubator. All the glassware and media used were sterilised in an autoclave at 121°C

200 for 20 min.

2.4.1 Minimum inhibitory concentration (MIC)

202 The antibacterial properties of the nanomaterials were tested against SRB after 14
203 days of anaerobic incubation at 30°C (Kamli et al., 2021). Minimum inhibitory
204 concentration (MIC) is the lowest concentration of BNPs that can completely inhibit
205 the visible growth of SRB isolated from oilfield-produced water. Two-fold serial
206 dilutions of BNPs were performed in Postgate'C medium (100, 50, 25, 12.5, 6.25, 3.12,
207 1.56 and 0 µg·mL^{-1}) at a volume of 200 µL·well^{-1}, and 10 µL of the standardised
208 inoculum was inoculated per well. Experiments were carried out in triplicate, including
209 a positive control with BNPs in nutrient solution not inoculated with SRB and negative
210 control with BNPs in nutrient solution not inoculated with SRB. The optical density at
211 600 nm was measured after 7 days and corrected by subtracting the background
212 absorbance of the positive control.

2.4.2 Lactate dehydrogenase (LDH) assay

214 The integrity of the cell membrane was examined by measuring the release of
215 lactate dehydrogenase (LDH) (Bezza et al., 2020). After MIC assay, 100 µL of the cell
216 suspension was collected and cells were lysed according to the procedure of the Lactate
217 Dehydrogenase (LDH) Assay Kit. The absorption peak at 450 nm was measured to
218 calculate the cytotoxicity percentage:

$$Cytotoxicity(\%) = \frac{(LDH\ release\ from\ samples - LDH\ background)}{(Maximum\ LDH\ release - LDH\ background)} \times 100\% \quad (1)$$

220 where *LDH realease from samples* refers to the absorbance at 450 nm of the product at
221 which the lysis of cells in the sample releases LDH to catalyse the reaction of lactic
222 acid to pyruvate with 2,4-dinitrophenylhydrazine. *LDH background* means the
223 absorbance at 450 nm of the pyruvate content detected in the medium of an
224 uninoculated cell culture. *Maximum LDH release* refers to the absorbance at 450 nm of
225 the pyruvate produced by LDH in an untreated sample.

2.4.3 MTT assay

227 3-(4,5-Dimethyl-2-Thiazolyl)-2,5-diphenyl tetrazolium bromide (MTT) staining
228 assay was carried out to detect the effect of BNPs on the cellular activity of SRB
229 (Gurunathan et al., 2013). The cultures were inoculated in 96-well plates at a density of
230 105 cells·mL^{-1} and treated with doubling dilution BNPs (0, 1.56, 3.12, 6.25, 12.5, 25,
231 50 and 100 µg·mL^{-1}) for 96 h at 30°C. The deteriorated medium was then replaced with
232 100 µL of the fresh deaerated medium. All media were aspirated after 96 h of incubation

233 and injection of 20 µL of PBS in 0.5 mg·mL^{-1} MTT solution for 4 h at 30°C. About 150

234 µL of DMSO (dimethyl sulfoxide) was added and incubated for another 4 h. Optical

235 density at 585 nm was recorded with a microplate reader after vigorous agitation of

236 each well. Cell viability was calculated as follows:

237

$$Cellular\ Vitality = \frac{NPs\ treated\ cells}{Untreated\ cells} \qquad (2)$$

238 where *NPs treated cells* is the absorbance at 585 nm of different concentrations of BNPs

239 treated samples stained by MTT. *Untreated cells* is the absorbance at 585 nm of SRB

240 cultures under normal conditions stained by MTT.

241 **2.5 Corrosion inhibition test**

242 **2.5.1 Adhesion test**

243 Crystalline violet assay was used to assess and quantify the inhibitory properties

244 of BNPs on SRB biofilm biomass (Shaker and Shaaban, 2017). A Q235 steel carbon

245 steel sheet was placed in 10 mL of Postgate'C medium. The medium was inoculated

246 with 0.5 mL of SRB to form biofilms according to the concentration of BNPs in the

247 MIC assay (Chávez-Andrade et al., 2019). After 7 days of incubation at 30°C, the

248 contents of the anaerobic flask were aspirated. The inner walls of the anaerobic flask,

249 and the carbon steel surface were flushed twice with 10 mL of sterile phosphate-

250 buffered saline (PBS, pH 7). Positive control with BNPs in the medium not inoculated

251 with SRBs and negative control with SRBs in the medium not inoculated with BNPs

252 were included. The attached biofilm in each flask was fixed with glutaraldehyde for 15

253 minutes. The biofilm was stained with crystal violet (1%, w/v). The anaerobic flask and

254 carbon steel surfaces were flushed with distilled water dried at 50°C. Glacial acetic acid

255 (33%) was used to dissolve the adherent bacteria. OD$_{490\ nm}$ was recorded in UV/vis to

256 quantify the amount of biofilm formed. The inhibition ratios of biofilm formed were

257 calculated as follows:

258

$$Inhibition\ rate = \frac{\text{OD}_{Untreated\ cells} - \text{OD}_{Nano-treated\ cells}}{\text{OD}_{Untreated\ cells}} \qquad (3)$$

259 where *OD$_{Untreated\ cells}$* is the absorbance at 490 nm of cell membranes in cultures without

260 BNPs after staining with crystal violet. *OD$_{Nano-treated\ cells}$* means the absorbance at 490

261 nm of cell membranes present in samples treated with different concentrations of BNPs

262 after staining with crystal violet.

263 **2.5.2 Weight-loss method**

264 The corrosion samples of Q235 steel were placed in 10 mL of anaerobic culture

265 flasks, and the samples were weighed (with an accuracy of 0.1 mg). Every 0.5 mL of

266 SRB cultures were added with 0, 3, 6 and 9 $\mu g \cdot mL^{-1}$ ginger extract-synthesised BNPs

267 in 10 mL of Postgate'C medium. The carbon steel was collected after incubation for 3,

268 6, 9, 12 and 15 days. The surface corrosion products were treated with a pickling

269 solution prepared with 12% HCl and 2% urotropine. The sample surface was flushed

270 with sterile deionised water and wrapped with filter paper to dry to constant weight at

271 60°C. The pieces were placed in a desiccator for cooling to room temperature and

272 weighed again. The following equation was used to calculate corrosion rate ($g \cdot m^{-2} \cdot h^{-1}$):

273
$$Cr = \frac{W_0 - W_i}{S \times t} \tag{4}$$

274 where W_0 is the original weight of the sample (g); W_i is the final weight (g); S is the

275 exposed surface area of the sample (m^2); and t is the corrosion time (h).

2.5.3 Corrosion morphology

277 SRB cells were treated with BNPs at a concentration of 6 $\mu g \cdot mL^{-1}$ for 72 h at 30°C.

278 SEM (Zeiss merlin compact) and transmission electron microscope (TEM, HITACHI

279 HT7700) were used to observe the corrosion of the carbon steel surface and the damage

280 of SRB cells before and after BNP treatment.

2.6 Statistical analysis

282 Student's t-test was used to measure statistical correlation and significance. $p <$

283 0.05 was set as the limit for significance after analysis using two-sample t-test and two-

284 tailed distribution.

285

3. Results and discussion

3.1 Characterization of BNPs

288 Particle size analysis showed the majority of particle size distribution of BNPs of

289 approximately 34 nm (**Table 1**), indicating the ability of the ginger extract to reduce

290 metal ions. Nanoparticles with particle sizes within 20–50 nm accounted for 89.94% of

291 the total particle size, indicating the uniformity and monodispersity of BNPs. Despite

292 most of the synthesised nanoparticles having a small particle size, SEM showed that

293 nanoparticles with a particle size around 79 nm had a different shape. The synthesised

294 BNPs were formed rapidly within 60 minutes and remained stable even after 24 hours.

295 The stability of the synthesised BNPs extracted from ginger was verified by UV-visible

296 spectroscopy which showed an absorption peak at about 295 nm (**Fig. 1**), which can be

297 due to the absorption of BNPs (Merugu et al., 2021). The width of the absorption spectra

298   was attributed to the multi-crystalline properties of Ag/Cu BNPs, and the extracts

299   showed reduce nanoagglomeration.

300   **Table 1** Particle size distribution of Ag/Cu BNPs synthesised from ginger rhizome extracts.

Particle size(μm)	Cum%	Diff%
0 ~ 0.02	0	0
0.02 ~ 0.05	89.94	89.94
0.05 ~ 0.1	6.26	96.2
0.1 ~ 0.2	0.46	96.66
0.2 ~ 0.5	2.29	98.95
0.5 ~ 1	0.49	99.44
1 ~ 2	0.56	100
< 2	0	100

301
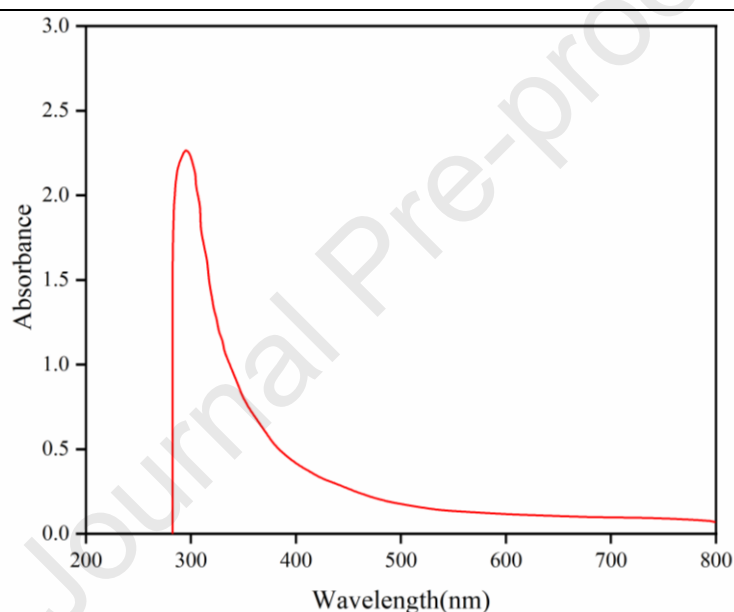
302   **Fig. 1.** UV-Vis spectrogram of Ag/Cu BNPs. Appearance of an absorption peak at 295 nm indicates

303   the synthesis of Ag/Cu BNPs.

304   The synthesis of small-sized BNPs with uniform particle size is the key point to

305   enhance the corrosion inhibition effect of ginger extract and inhibit the growth of SRB.

306   SEM analysis was used to investigate the size, shape and morphology of BNPs

307   synthesised from the ginger extract. **Fig. 2** (A, B) shows the electron microscope image

308   at 40,000x magnification. BNPs with particle sizes below 50 nm were spherical, and

309   BNPs with particle sizes between 50–100 nm were rhombic and lamellar.

310   Agglomeration was not observed in any of these particles. The EDS spectra confirmed

311   the weight percentages of Ag and Cu in Ag/Cu BNPs as 42.88% and 6.70% and the

312   atomic ratios as 10.23% and 2.72%, respectively. The EDS spectrum and SEM images

313   demonstrated the potential of the reducing properties of ginger extract in the synthesis

314   of BNPs.

315
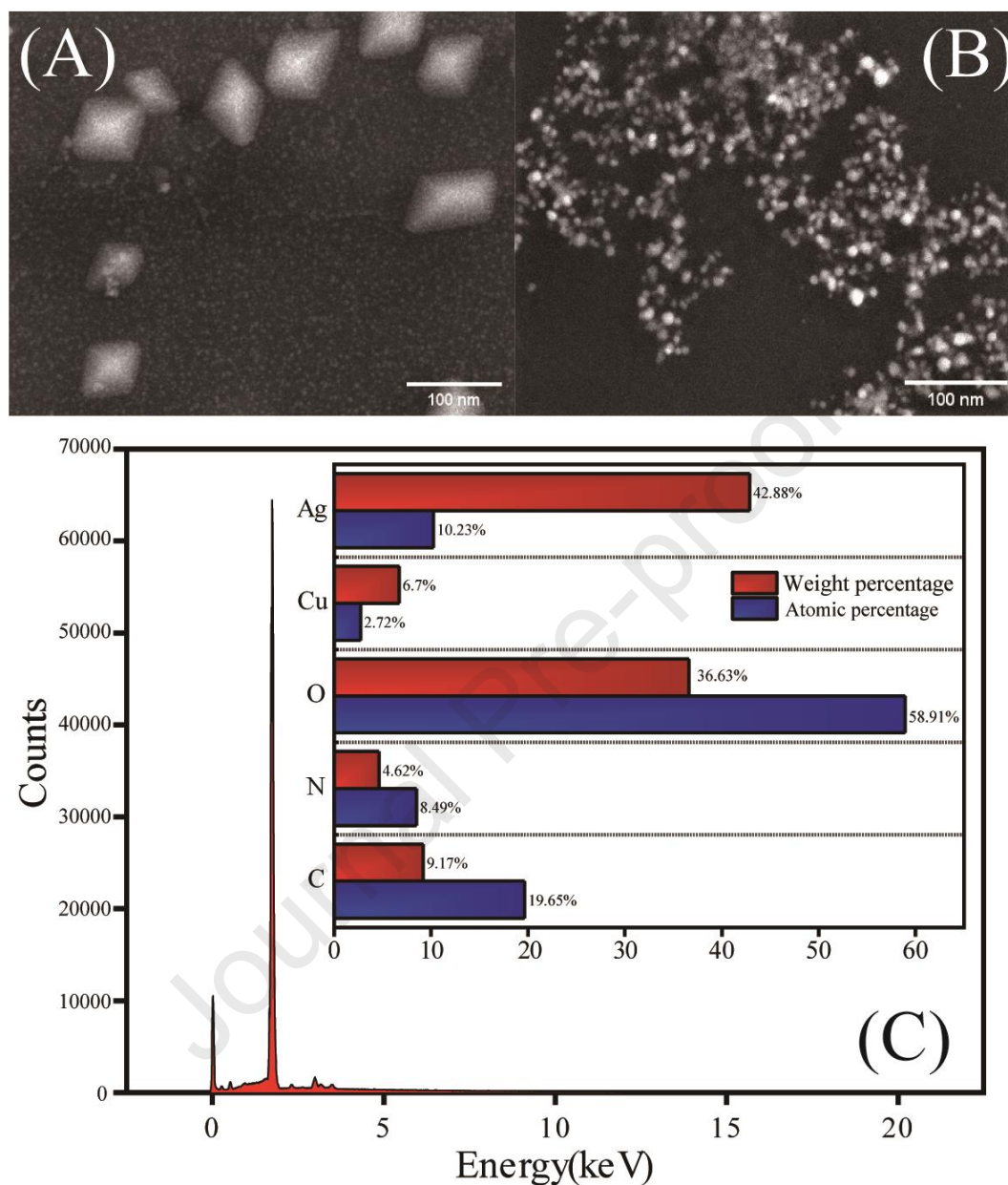
Fig. 2. Representative SEM images of Ag-Cu NPs synthesised from the ginger extract and EDX
patterns. (A, B) Synthesised Ag/Cu BNPs had circular and rhombic shapes at 40,000x magnification;
(C) Synthesised nanoparticles containing Ag and Cu.

319   The maintenance of the long-term stability of nanoparticles is as important and

320   critical to their efficient antimicrobial and catalytic applications as their dimensional

321   morphology (Merugu et al., 2021). Therefore, the conditions for the synthesis of

322   nanomaterials were optimised and analysed in this experiment to investigate the effects

323   of the precursor concentration, the volume ratio of precursor to extract, reaction time

324   and reaction temperature on the particle size morphology as well as the stability of

325   BNPs. The temperature had the greatest effect on the size of the synthesised
326   nanoparticles. The order of influence of the factors on the synthesis of NPs from the
327   ginger extract was temperature > precursor concentration > volume ratio of precursors
328   to extract > reaction time. Increasing the reaction temperature led to larger synthesised
329   nanoparticle size, while prolonging the reaction time had almost no significant effect
330   on nanoparticle size and amount produced.

331   The FTIR spectra showed strong absorption peaks at 3416, 2927, 1628, 1565, 1409
332   and 651 cm^{-1}, indicating the presence of phytochemicals. This finding could be the
333   reason for the synthesis of BNPs (**Fig. 3**). Ginger extracts are mainly composed of
334   gingerols and gingerones (Dalsasso et al., 2022). **Fig. 3** presents the structural formulae
335   of the main components. The figure shows the deformation vibration of -CH=CH-
336   (trans) at 3416 cm^{-1}, the stretching vibration of -CH at 2927 cm^{-1}, and the stretching
337   vibration of C=O at 1628 cm^{-1} (Lee et al., 2019). The absorption band around 1565 cm^{-1}
338   is the vibrational absorption band of the benzene ring molecular framework, and the
339   vibrational absorption band of 1,3,5 trisubstituted benzene rings at 1385, 870 and 775
340   cm^{-1}. The functional groups information in the FT-IR spectra of the ginger extracts were
341   correlated well with the chemical structures of gingerone and gingerol. The ginger
342   extract contains polar groups that are protonated easily in acidic solutions, such as
343   hydroxyl, carbonyl and benzene rings. The negatively charged steel surface in a
344   corrosive environment can adsorb the protonated ginger extract by electrostatic action
345   (Liu et al., 2019). Oxygen atoms in the ginger extract can form coordination bonds with
346   iron atoms resulting in an empty d orbitals that are not occupied, forming well-adsorbed
347   films on the steel surface after chemisorption (Loto et al., 2020). The oxygen-containing
348   polar groups in the ginger extract have a large number of lone pairs of electrons, which
349   can form a chelate with Fe^{2+} in the solution to adsorb on the metal surface and enhance
350   corrosion inhibition (Farmoudeh et al., 2021). The changes in the spectra before and
351   after the synthesis of nanoparticles were indicted by the new characteristic peaks at
352   2300 and 1761 cm^{-1} (El-Refai et al., 2018). This observation is attributed to the variation
353   in the position of the aromatic hydrogen atom on the substituted aromatic ring, causing
354   an extraplanar deformation vibration in the region between 2000 and 1700 cm^{-1}
355   (Ramzan et al., 2022).
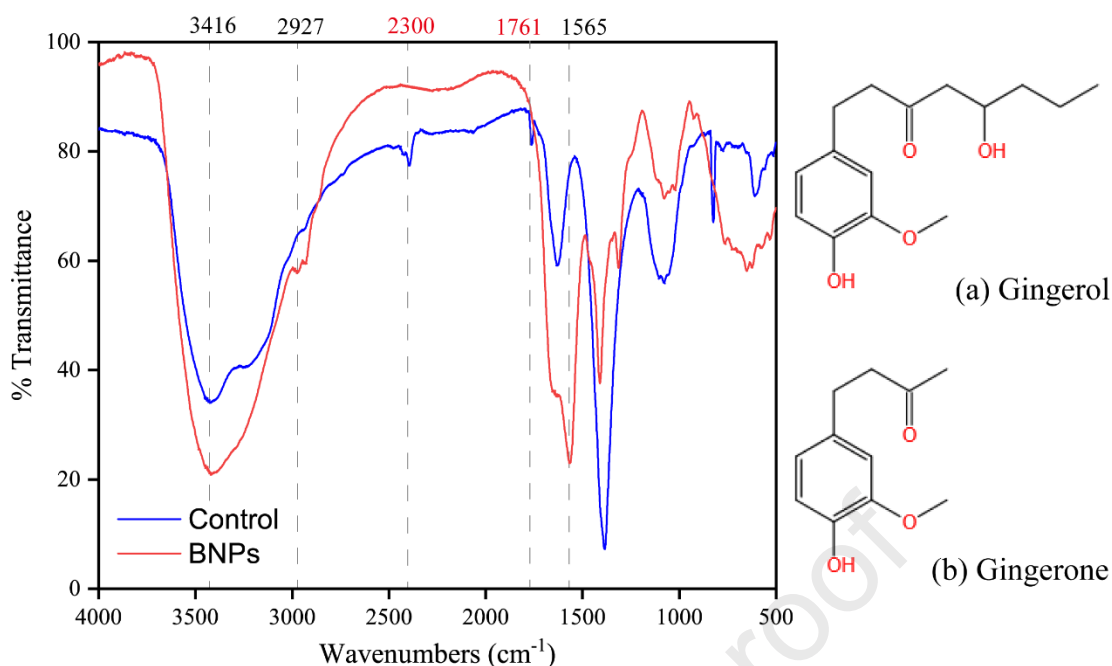
Fig. 3. FTIR spectra of ginger extract and its synthesised Ag/Cu bimetallic nanoparticles. The diagram on the right gives the chemical formula for the main component of gingerol.

The intensity of the conjugated olefin peak around 1600 cm^{-1} significantly decreased, which might be due to the fact that the double bond played a major role in the reduction of metal ions. The substitution of the hydrogen atoms on the benzene ring and the structural deformation of the conjugated olefin are related to the reduction of the metal. Alternatively, the site may bind to a zero-valence metal particle to prevent its growth after nucleation and act as a capping agent during nanostabilisation. It provides sufficient evidence that ginger extract can be used as a material for the synthesis of BNPs without additional chemical catalysts or dispersing substances in an environmentally friendly manner.

3.2 Antibacterial activity

3.2.1 Minimum inhibitory concentration (MIC)

The antibacterial activity of Ag/Cu BNPs synthesised from the ginger extracts against SRB was evaluated by standard doubling dilution. The dose-dependent antibacterial activity of BNPs was demonstrated by incubating the cultures at 30°C for 7 days. Optical density (OD) of the cultures was recorded at 600 nm. **Fig. 4** presents the growth of SRB in the absence of BNPs synthesised by ginger. SRB can be grown at concentrations below 12.5 μg·mL^{-1} of BNPs synthesised by ginger. Nevertheless, bacterial growth was significantly inhibited at 12.5 μg·mL^{-1} BNP. Hence, BNPs synthesised by the ginger extract inhibited the growth of SRB bacteria at 12.5 μg·mL^{-}

378   [1]. The growth of SRB-treated with 6.25 μg·mL^{-1} BNPs was slightly lower than the cells

379   in the control group, but no significant inhibitory effect was observed. Consequently,

380   the MIC of BNPs synthesised by the ginger extract was 6.25 μg·mL^{-1}, at which the SRB

381   bacteria were sensitive to BNPs synthesised by the ginger extract. There was no

382   significant change (P>0.05) observed in the antibacterial activity of BNPs synthesized

383   from ginger extracts against SRB in the three sets of parallel tests, indicating that BNPs

384   have a stable inhibitory effect on SRB.

385   The antibacterial properties of NaClO solution and silver nanocluster hydrogel for

386   SRB were studied by Yang et al. (2020). Both 225 μg·mL^{-1} NaClO solution or 18.75

387   μg·mL^{-1} silver nanocluster hydrogel had a significant antibacterial effect on SRBs.

388   However, this method not only requires the use of higher concentrations of chemical

389   reagents, but can also be harmful to the environment. An increasing number of research

390   has been carried out using nanomaterials to treat drug-resistant SRBs in oil fields

391   because chemical inhibitors are susceptible to drug resistance and hazardous to the

392   environment (Karimi-Maleh et al., 2021). In contrast, the MIC of the BNPs synthesised

393   in this experiment is only 12.5 μg·mL^{-1} and can inhibit the corrosive effect of SRBs by

394   blocking their colonisation of the carbon steel surface, which is a better response to the

395   development of bacterial resistance.
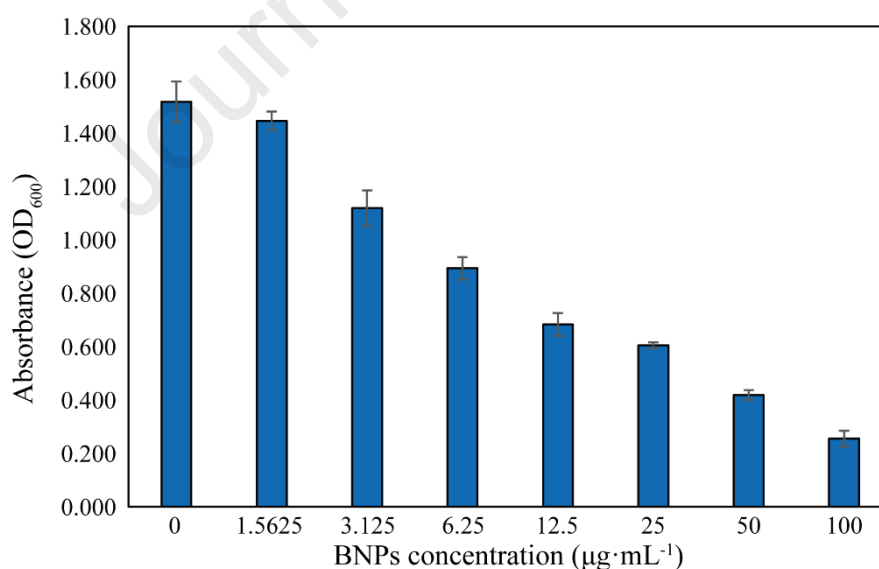
396

397   **Fig. 4.** Growth of SRB culture mixtures in media containing BNPs synthesised from ginger extract

398   at different concentrations. Data represent the mean ± SD of three different experiments carried out

399   in triplicate.

400   Monometallic AgNPs synthesised using Tulsi extract and quercetin in earlier

401   reports had higher MIC value (low inhibition efficiency) of 150 μg·mL^{-1} against Gram-

402   negative strains of *Escherichia coli* (Jain and Mehata, 2017). Bimetallic nanomaterials

403   have been used in recent years by Kamli et al. (2021). In brief, 6.0–64.0 µg·mL^{-1} Ag/Cu

404   bimetallic NPs were found to have antifungal activity against drug-resistant *Candida*.

405   As ginger extract has been applied in many antibacterial aspects, ginger extract alone

406   at 7.6–8.3 mg·mL^{-1} showed antibacterial activity against *Streptococcus mutans*,

407   *Lactobacillus acidophilus*, *Staphylococcus aureus*, *Pseudomonas aeruginosa*,

408   *Actinomyces viscosus* and *Veilonellaalca ligens* (Saleh et al., 2018). Therefore, ginger

409   extract and the bimetallic nano had combined antibacterial activity in this experiment,

410   which can effectively reduce the dose and reach a improved antibacterial effect. In

411   addition, factors such as shape and size of the nanoparticles, type of stabiliser, growth

412   phasing of the inoculum size and type of microbial strain are critical in the

413   determination of MIC values (Akter et al., 2018).

414   **3.2.2 Lactate dehydrogenase (LDH) assay**

415   The release of lactate dehydrogenase (LDH) was evaluated by a cytotoxicity test

416   based on membrane integrity. **Fig. 5** illustrates the relationship between the

417   concentration of BNPs and the release of LDH from SRB cells. For BNPs less than 6.25

418   µg·mL^{-1}, the LDH released by SRB bacteria increased gradually in a dose-dependent

419   manner. The dose of 3.125 µg·mL^{-1} caused 42.97% of LDH release. LDH release no

420   longer changed significantly ($p > 0.05$) when the concentration of BNPs increased,

421   remaining at 46% to 48%. **Fig. 5** indicates that the increase in the BNP concentration

422   did not lead to any further increase in LDH release. Regardless of the concentration of

423   BNPs increased, the toxic effect on cells remained approximately 50%. In comparison

424   with the results of the MTT assays, BNPs at doses of 3.125–25 µg·mL^{-1} had limited

425   inhibition effects on cellular activity but had the same cytotoxicity with higher doses of

426   BNPs. In general, the exposure of NPs to the bacterial membrane directly led to the

427   leakage of intracellular components (Lahiri et al., 2021). Ginger extract has been shown

428   to exhibit strong DNA damage protective activity (Bhattacharya et al., 2022). The toxic

429   effects of BNPs on cells could originate from the release of Ag$^+$ and Cu^{2+} ions that bind

430   to the cell membrane proton pump proteins and enzymes to form stable bonds, resulting

431   in cell viability and ultimately death.

432
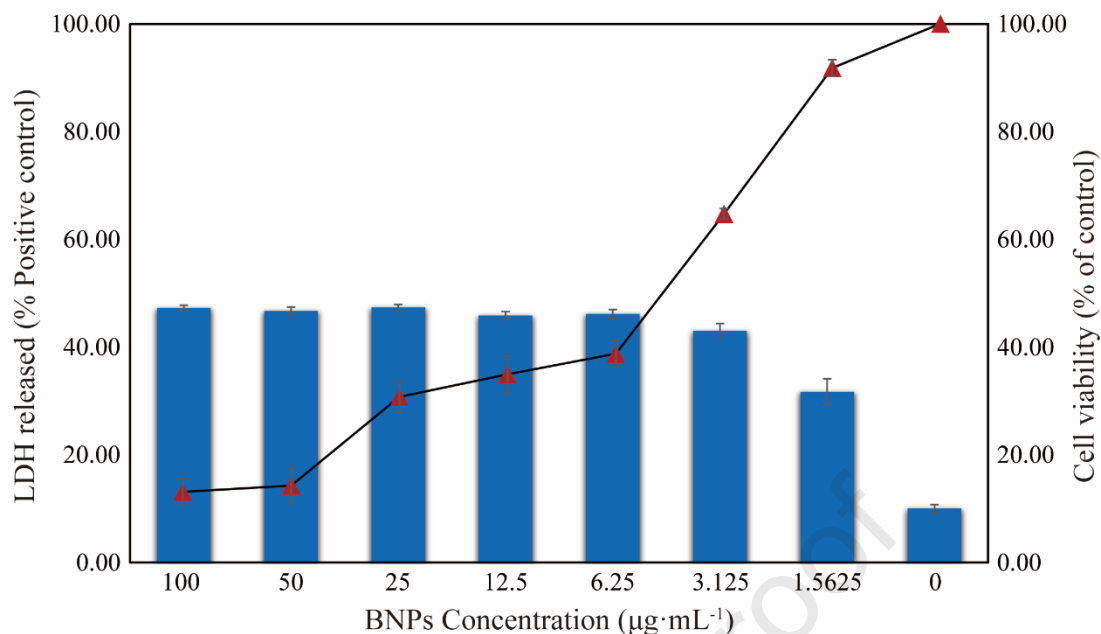
Fig. 5. The linear presents the effect of SRB on cell viability ssessed by MTT reduction assay after exposure to different concentrations of BNPs synthesised from ginger extract for 72 hours. Columns indicate the cytotoxicity of BNP synthesised from ginger extract to SRB bacteria as assessed by lactate dehydrogenase (LDH) release after incubation at 30°C for 72 hours. Results are presented as the mean ± SD of three independent experiments performed in triplicate.

3.2.3 MTT assay

SRB are prokaryotes and do not possess mitochondria. The MTT dye in this experiment is staining for succinate dehydrogenase in the electron transfer process that occurs in the cytoplasmic membrane (Gurunathan et al., 2013). **Fig. 5** shows the cell viability assessed in the MTT assay after treatment of SRB cells with BNPs synthesised from the ginger extract. The viability of these cells significantly decreased compared with that of the control cells. The results of the MTT viability assay indicated that the degree of completion of the respiratory chain of SRB cells decreased obviously when the cells were exposed to BNPs synthesised from the ginger extract for 72 hours. The cell viability decreased by 58.69% at BNP concentrations of 6.25 $\mu g \cdot mL^{-1}$ and by 82.15% at 50 $\mu g \cdot mL^{-1}$. If the treatment concentration of BNPs would be increased persistently, then the cell viability would not decrease further. **Fig. 6** (A) shows the result of decreased cell viability, the higher the concentration of BNPs the fewer pitting pits there are on the surface of the carbon steel after treatment. The SEM image of the deposit in **Fig. 6** (B) illustrates the rupture and reduction in size of the bacterial cells within the deposit produced by the BNPs-treated SRB.
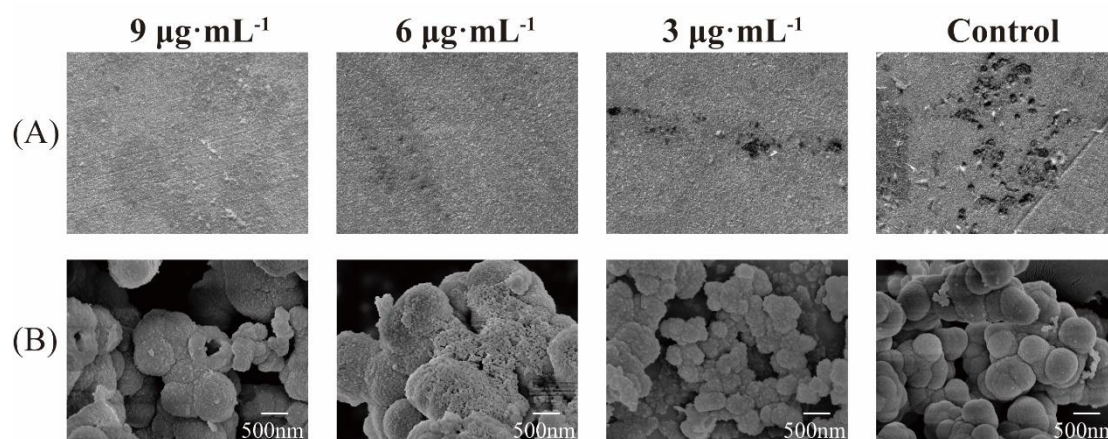
Fig. 6. (A) Optical microscope image of the surface on carbon steel after corrosion by SRB. (B) SEM image of the collection of deposited fouling produced by SRB.

The determination of the half-maximum (50%) inhibitory concentration (IC_{50}) is essential to comprehensively determine the efficacy measures of antagonist drugs in pharmacological studies (Aykul and Martinez-Hackert, 2016). AgNPs have broad-spectrum antimicrobial activity against cells of Gram-negative bacteria (*Pseudomonas aeruginosa* CB1) and Gram-positive bacteria (*Bacillus subtilis* CN2). Notably, a significant change in cellular activity ($p<0.05$) was induced when the concentration of BNPs was increased from 3.125 $\mu g \cdot mL^{-1}$ to 6.25 $\mu g \cdot mL^{-1}$ and from 25 $\mu g \cdot mL^{-1}$ to 50 $\mu g \cdot mL^{-1}$. Furthermore, the IC_{50} of BNPs synthesised from the ginger extract was 6.26 $\mu g \cdot mL^{-1}$ for the inhibition of SRB growth, which is slightly higher than the previously reported broad-spectrum inhibition value of AgNPs (Bezza et al., 2020). These findings may be due to the availability of the DA-G20 detoxification mechanism in SRB. This mechanism prevents metal ions from entering the cell by down-regulating several inorganic ion transport protein complexes and up-regulating specific transport protein complexes. The initiated transport of metal ions out of cells can buffer the oxidative stress associated with heavy metals (Tripathi et al., 2022). As a result, metal ions can be transferred by SRB through this metabolic mechanism at lower concentrations of BNPs, minimizing the damage to cells as well. As the treatment concentration of BNPs gradually increased, the rate of their combination exceeded the regulatory capacity of the cells after reaching 6.26 $\mu g \cdot mL^{-1}$. A significant inhibition of SRB cell activity was observed. The cell activity decreased by almost 90% at the treatment concentration of 50 $\mu g \cdot mL^{-1}$, which may be due to the fact that the specific metabolites synthesised during the pre-transport of metal ions are still available in the environment even though some of the cells already died with increasing concentration. The detoxification

480   mechanism of SRBs that BNPs can resist implies that plant-based corrosion inhibitors

481   have the potential to reduce the enrichment of ferrous sulphide precipitation during

482   production.

483   **3.3 Corrosion Inhibition Applications**

484   The application of ginger-synthesized BNPs for corrosion inhibition, based on

485   their previously demonstrated properties in the inhibition of SRB-induced corrosion of

486   carbon steel in oilfield produced water, was demonstrated by adhesion assays and

487   weight loss tests. In the application example presented here, BNPs synthesised from

488   ginger extracts managed to reduce the adhesion of SRB cells on the surface of carbon

489   steel by 65% and decreased the rate of weight loss of carbon steel by 77% under the

490   conditions simulated in the laboratory.

491   **3.3.1 Adhesion test**

492   Adhesion assay was used to demonstrate the inhibition of biofilm formation by

493   SRB with BNPs synthesised from the ginger extract. ZnO nanomodified with carbon

494   steel surface was applied to inhibit SRB adhesion and corrosion on carbon steel surface

495   by Li et al. (2022). The modified ZnO particles with a larger specific surface area

496   produced more Zn^{2+}, thereby limiting the growth of SRB. In addition, chitosan-zinc

497   film modification of carbon steel surface was used by Zhai et al. (2018) to inhibit SRB

498   adhesion. They proposed that the composite chitosan did not change the cathodic and

499   anodic reactions of the zinc film corrosion process. However, the corrosion ability of

500   SRB agents was reduced slightly, and the adhesion of bacteria was inhibited. This

501   finding indicated that the material modification did not inhibit the metabolic process of

502   SRB but only reduced the adhesion on the surface of carbon steel. These methods do

503   not apply to old oil pipelines that had been corroded. Therefore, the effects of BNPs

504   synthesised from ginger extract on the adhesion of SRBs on the surface of ordinary

505   carbon steel in the environment were investigated in this paper.

506   **Fig. 7** shows that BNPs synthesised from ginger extracts remarkably inhibited the

507   formation of biofilms in cultures. The degree of inhibition of biofilm formation at lower

508   concentrations of BNPs (~12.5 $\mu g \cdot mL^{-1}$) was approximately 37%, and the degree of

509   inhibition did not change significantly (p>0.05) with variations of BNPs concentration.

510   Increasing the BNP concentration above 50 $\mu g \cdot mL^{-1}$ can effectively inhibit biofilm by

511   65%. This finding implies that the low concentrations of BNPs have no dose-dependent

512   effect on the adhesion activity of SRB, while a high concentration of BNPs can reduce

513   the adhesion activity of SRB on the surface of ordinary Q235 carbon steel. Reducing

514   the adhesion of SRB to the surface of carbon steel is of great importance in protecting

515   the production environment and preventing blockages in oil pipelines.
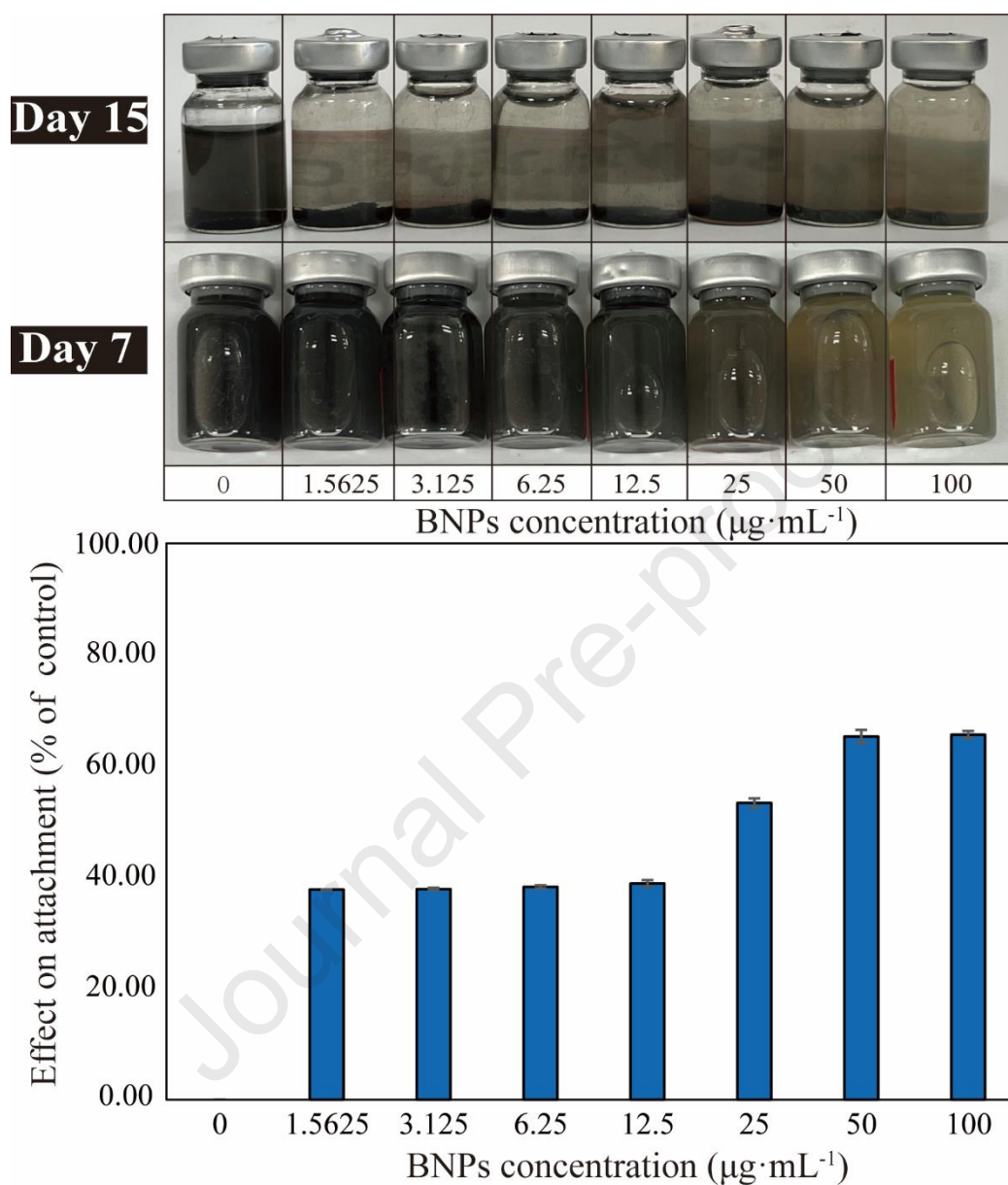
516

517   **Fig. 7.** Effect of BNPs on SRB cell attachment behaviour compared with untreated control bacteria.

518   Results are expressed as the mean ± SD of three independent experiments performed in triplicate.

519   **3.3.2 Weight-loss analysis**

520   The weight loss rate of carbon steel during a 15-day incubation period was

521   analysed for the corrosion behaviour of SRB (Hansen et al., 2021). As the SRB is

522   caused by the corrosion features for pitting, according to the American Association of

523   Corrosion Engineers (NACE International) current standards can be divided into four

524   categories of slight corrosion, moderate corrosion, severe corrosion, and extremely

525   severe corrosion (Zhai et al., 2018). The corrosion rate is below 0.127 mm·a^{-1} for light

526 corrosion and above 0.308 mm·a^{-1} for extremely serious corrosion. The weight loss of

527 carbon steel at 30°C for 15 days was recorded during this period, and the change in the

528 corrosion rate is shown in **Fig. 8**. The SRBs in the group without BNPs were incubated

529 for 150 h before reaching the logarithmic growth phase. The corrosion rate increased

530 from the initial 0.101 mm·a^{-1} to 0.453 mm·a^{-1}, which occurred in extremely severe

531 corrosion. By contrast, the group treated with BNPs maintained the carbon steel

532 samples in a slightly corroded state throughout the period, with almost no weight loss

533 observed. The rate of carbon steel weight loss in the group treated with BNPs after one

534 week of incubation was significantly lower than in the untreated group ($p < 0.05$), which

535 implies that BNPs are effective in reducing the loss of carbon steel mass due to SRB

536 growth. The weight loss of carbon steel became more effective as the concentration of

537 BNPs increases. This finding indicates a dose-dependent relationship between the

538 concentration of BNPs and the corrosion rate of SRB. Corrosion inhibition remained

539 positive for over 15 days after treatment. The effect of concentration on the time of

540 valid corrosion inhibition can be further studied.
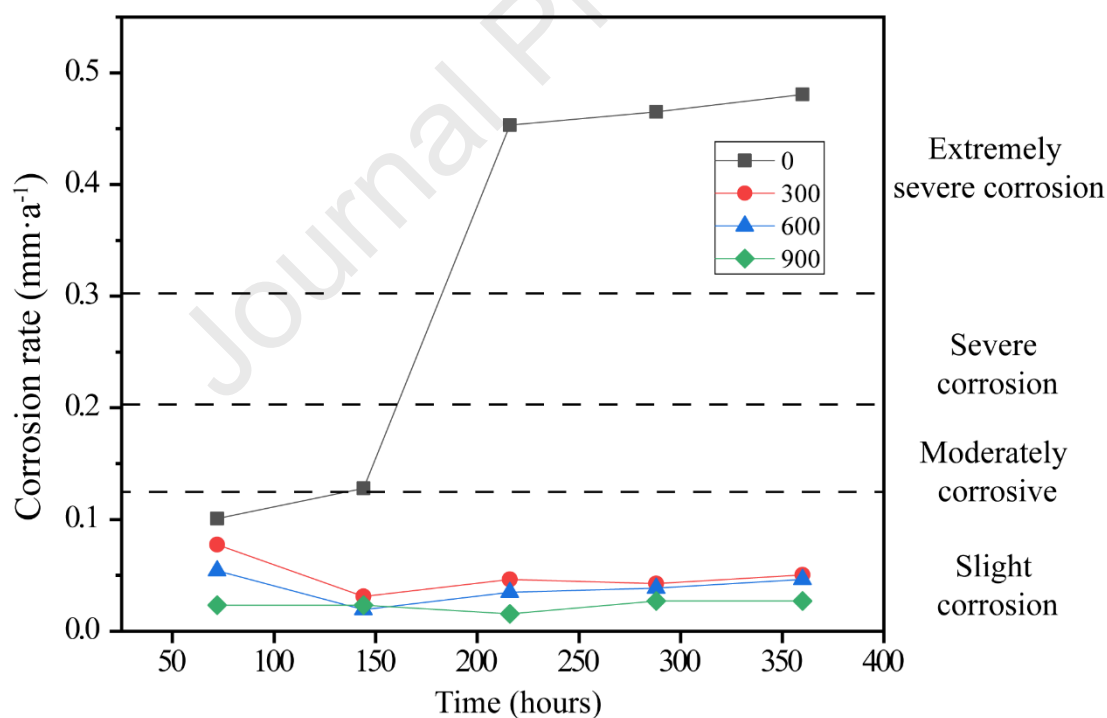
541

542 **Fig. 8.** Corrosion of carbon steel by SRB at 30°C and weight loss rate of carbon steel after treatment

543 with different concentrations of BNPs.

544 Ginger extract can inhibit corrosion on carbon steel surfaces in an acidic

545 environment. The effect of ginger extract adsorption on the surface of carbon steel to

546 reach corrosion inhibition was reported by Fouda et al. (2013). And the corrosion rate

547   was reduced to 0.2 mm·a^{-1} by 2 μg·mL^{-1} of ginger extract was reported by Narenkumar

548   et al. (2017). The synergistic effect of ginger extract and BNPs in this application

549   reduced the corrosion rate by more than 77.7%, with a longer duration of action and

550   better corrosion inhibition than previous corrosion inhibition results.

551   **3.4 Corrosion inhibition mechanism**

552   Scanning electron microscopy (SEM) was used to observe the morphological

553   changes in the carbon steel surface after BNP treatment while Transmission electron

554   microscopy (TEM) was used to observe the ultrastructural details of SRB cells after

555   BNPs treatment to elucidate the mechanism of BNPs in corrosion inhibition. **Fig. 9** (a)

556   shows the carbon steel surface after inoculation with SRB cells for 15 days. The surface

557   of carbon steel became quite rough with many corrosion spots after cleaning the

558   corrosion products on the surface of carbon steel. Moreover, the corrosion points were

559   interconnected to form larger corrosion pits owing to the high concentration of the

560   inoculated SRB. By contrast, **Fig. 9** (b) shows that the carbon steel surface was

561   relatively smooth after treatment with 9 μg·mL^{-1} BNPs. Only few localised corrosion

562   spots were found on the treated surface, which indicates a uniform corrosion formed by

563   the water and the composition of the culture medium.

564
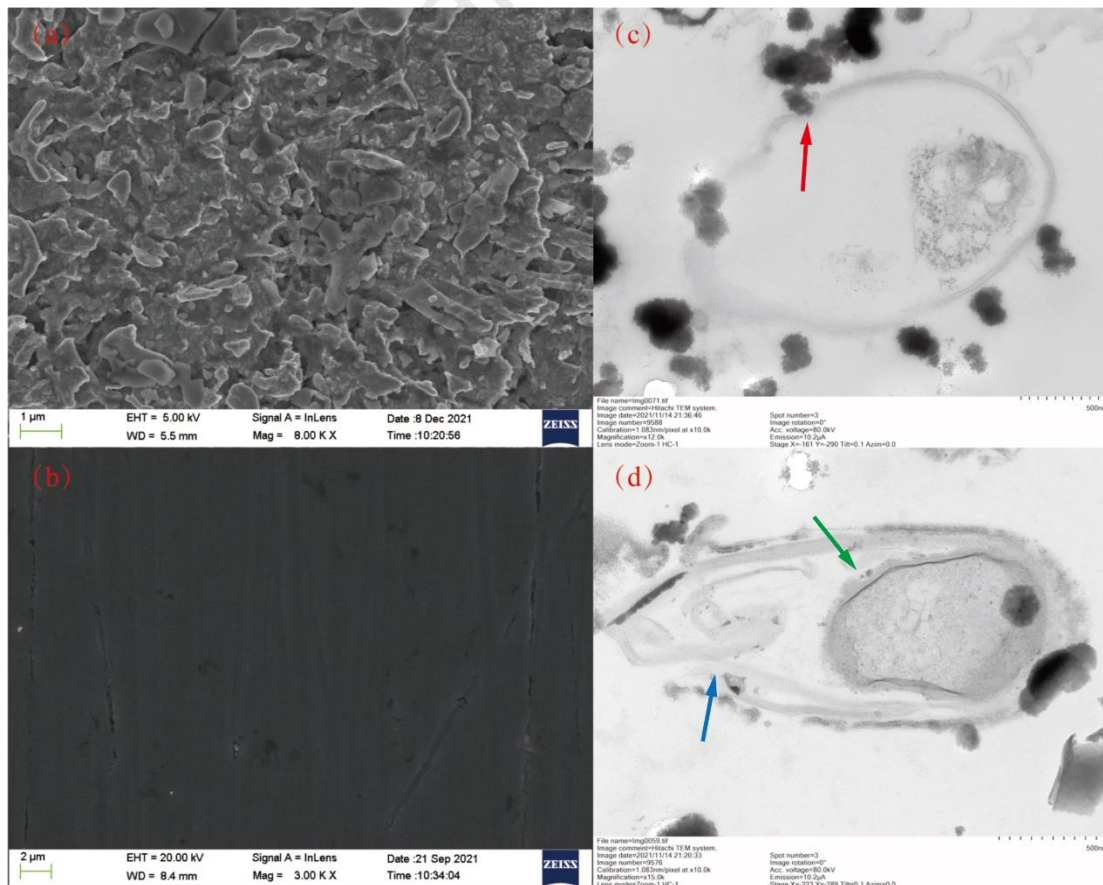
565   **Fig. 9.** SEM images of the carbon steel surface before (a) and after (b) BNP treatment and TEM

566   images of SRB cells before (c) and after (d) BNP treatment.

567   The corrosion products in the samples were collected and flushed with sterile PBS

568   buffer. SRBs were observed by TEM after immobilisation and drying to evaluate the

569   adsorption or internalisation of BNPs in the cells. **Fig. 9** (c, d) reflects the morphology

570   of SRB cells before and after BNP treatment. The SRB cells are normally oval in shape

571   and electron-dense and have an integrated surface. The cytoplasmic membrane is

572   uniformly distributed, and many corrosion metabolites are present on the surface as

573   well as in the periplasmic space. The yellow arrow indicates that the exocytosis of SRB

574   generated nanoscale corrosion products. The surface of SRB cells was treated with 6

575    $\mu g \cdot mL^{-1}$ BNPs, while craters appeared on the surface (blue arrows). The rupture of the

576   cells occurred, the membrane was folded inward, and BNPs bound to the exterior

577   membrane were adsorbed. Portions of BNPs were internalised and interacted with

578   intracellular components, causing the leakage of cytoplasm (green arrows).

579   Considerable loss of membrane integrity and severe damage to the cell structure were

580   detected compared with the untreated control. SRB treated with BNPs showed

581   cytomorphosis with a significant reduction of corrosive metabolites in the periplasmic

582   space. This finding suggests that BNPs can disrupt the cellular integrity of SRBs and

583   inhibit their corrosive behaviour. The inhibition of SRB growth allows for clean and

584   safe oilfield production.
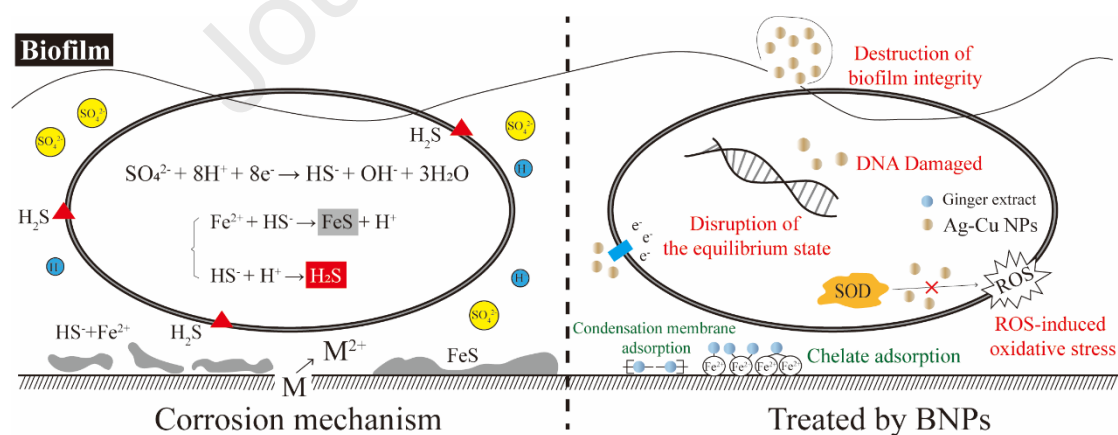
586   **Fig. 10.** Suggested mechanism of inhibition of SRB corrosion behaviour by BNPs synthesised from

587   the ginger extract.

588   BNPs synthesised from ginger extracts were demonstrated to have prominent

589   effects on inhibiting SRB growth, disrupting cell integrity, reducing cell activity, and

590   preventing cell adhesion on the metal surface. The main mechanism of the BNPs

591   synthesised from the ginger extract mixture is illustrated in **Fig. 10**. The incorporation

and internalisation of BNPs into cells were observed in TEM images. Bezza et al. (Bezza et al., 2020). reported that Ag NPs have broad-spectrum antimicrobial properties. This finding indicates that nanoparticles can be taken up by cells, resulting in too much reactive oxygen (ROS) and creating oxidative stress. The role of BNPs in disrupting the extracellular polysaccharides (EPS) of the biofilm substrate and preventing biofilm formation by destroying bacteria was reviewed by Lahiri et al. (2021). In addition, the macromolecules in the ginger extract can be chelated and adsorbed on the surface of carbon steel to enhance the corrosion inhibition effect (Subramanian et al., 2013). The inhibitory effect of BNPs on SRB might originate as follows: (1) DNA structural damage caused by nano-internalisation; (2) ROS caused by the inability of superoxide dismutase (SOD) destruction to scavenge free radicals; (3) disruption of the equilibrium state of the proton efflux pump and cytoplasmic leakage; and (4) prevention of biofilm production and inability of cells to establish drug resistance. These properties allow BNPs to effectively overcome the drug resistance generated by SRBs and can precipitate in aerobic and anaerobic bacteria to block the respiratory chain system of microorganisms (Parmar et al., 2022). Synergism is the process by which biological structures or chemical substances combine to produce greater effects than they would have alone (Ashishie et al., 2018). This work demonstrated that ginger extract synergistically functioned with BNPs to achieve better inhibition of SRB corrosion behaviour. In this way, the high surface energy of BNPs has a catalytic effect on the adsorption of ginger extract on the carbon steel surface. In summary, ginger extract synthesised BNPs can effectively inhibit the growth of SRB when BNPs affect the corrosion behaviour of SRB. Ginger extract can provide protection on the metal surface to slow down the occurrence of corrosion. This synergistic effect enables BNPs synthesised from ginger extracts to ensure oil and gas production safety and product purity by reducing the attachment of SRB biofilm and inhibiting SRB corrosion.

4. Conclusion and Recommendations

A biological and eco-friendly preparation of bimetallic nanoparticles that can effectively combat the resistance of sulphate-reducing bacteria was achieved in this paper. Corrosion inhibitors that can resist the adhesion of SRB on carbon steel surfaces and inhibit corrosion behaviour by disrupting their cellular structure were produced. The results showed that Ag/Cu BNPs with a particle size of ~34 nm were synthesized from ginger extract, and the composite system exhibited dose-dependent bactericidal

626 activity against SRB and could reduce the generation of ferrous sulphide precipitation

627 fouling. SRB activity in the culture can be significantly reduced by more than 50%,

628 which means that low concentrations of BNPs can already achieve the dual function of

629 corrosion inhibition of carbon steel and SRB growth inhibition. The notable aspect of

630 this method is the combination of the corrosion inhibiting activity of the ginger extract

631 with the antimicrobial activity of BNPs having a high surface energy, which kept the

632 carbon steel clean during the experiment and the SRB no longer produced FeS

633 precipitates and hydrogen sulphide gas. The corrosion rate of carbon steel was reduced

634 from 0.453 mm·a^{-1} to 0.05 mm·a^{-1} and the adhesion of SRB cells was reduced by 65%

635 during the application period. This demonstrates that BNPs synthesised from ginger

636 extracts can be applied to inhibit SRB-influenced corrosion processes in oilfield

637 produced water.

638 The synthesis of BNPs using plant extracts as corrosion inhibitors in oilfield

639 production has also been applied previously. This study innovatively uses a complex of

640 bimetallic nanoparticles and plant extracts to control microbial resistance affecting

641 oilfield pipeline corrosion, providing a new idea for solving production safety problems

642 such as pipeline leakage and hydrogen sulphide production. This creative and

643 environmentally friendly method of corrosion inhibitor production could have more

644 practical applications in the various production environments where SRBs are located.

645 Further study of the relationship between the treatment concentration of BNPs and the

646 effective corrosion inhibition time of SRBs could optimise the conditions for the

647 application of this inhibitor in the oilfield. Analysis of the biofilm components formed

648 by SRBs and the modulatory effect of BNPs on operators associated with quorum

649 sensing (QS) proteins during biofilm formation is significant for the improvement of

650 inhibition. All of these studies are important to promote the application of BNPs in

651 inhibiting pipeline corrosion in oilfield production.

652

Acknowledgements

656

References

658 Akter, M., Sikder, M.T., Rahman, M.M., Ullah, A., Hossain, K.F.B., Banik, S.,

659   Hosokawa, T., Saito, T., Kurasaki, M., 2018. A systematic review on silver

660   nanoparticles-induced cytotoxicity: Physicochemical properties and perspectives.
661   Journal of Advanced Research. 9, 1-16.

662   Arora, N., Thangavelu, K., Karanikolos, G.N., 2020. Bimetallic nanoparticles for
663   antimicrobial applications. Frontiers in Chemistry. 8, 412.

664   Ashishie, P., Anyama Ayi, A., Ayi, A., Oseghale, C., Adesuji, E., Hassan, L., 2018.
665   Green synthesis of silver monometallic and copper-silver bimetallic nanoparticles
666   using Kigelia africana fruit extract and evaluation of their antimicrobial activities.
667   International Journal of Physical Sciences. 13, 24-32.

668   Aykul, S., Martinez-Hackert, E., 2016. Determination of half-maximal inhibitory
669   concentration using biosensor-based protein interaction analysis. Analytical
670   Biochemistry. 508, 97-103.

671   Babaeekhou, L., Ghane, M., 2021. Antimicrobial activity of ginger on cariogenic
672   bacteria: molecular networking and molecular docking analyses. Journal of
673   Biomolecular Structure & Dynamics. 39 (6), 2164-2175.

674   Basavegowda, N., Baek, K.-H., 2021. Multimetallic nanoparticles as alternative
675   antimicrobial agents: challenges and perspectives. Molecules. 26 (4), 912.

676   Bezza, F.A., Tichapondwa, S.M., Chirwa, E.M.N., 2020. Synthesis of biosurfactant
677   stabilized silver nanoparticles, characterization and their potential application for
678   bactericidal purposes. Journal of Hazardous Materials. 393, 122319.

679   Bhattacharya, E., Pal, U., Dutta, R., Bhowmik, P.C., Mandal Biswas, S., 2022.
680   Antioxidant, antimicrobial and DNA damage protecting potential of hot taste
681   spices: a comparative approach to validate their utilization as functional foods.
682   Journal of Food Science and Technology. 59 (3), 1173-1184.

683   Birk, S.E., Boisen, A., Nielsen, L.H., 2021. Polymeric nano-and microparticulate drug
684   delivery systems for treatment of biofilms. Advanced Drug Delivery Reviews. 174,
685   30-52.

686   Bolaji, T.A., Oti, M., Abu, G., Onyekonwu, M., 2019. Biogenic sulfide production in
687   offshore petroleum reservoirs undergoing waterflooding. Petroleum and Coal. 61
688   (5), 1144-1157.

689   Cai, H., Wang, P., Zhang, D., Wang, Y., Li, E., 2021. An intelligent self-defensive
690   coating based on sulfide ion responsive nanocontainers for suppression of
691   microbiologically influenced corrosion induced by sulfate reducing bacteria.
692   Corrosion Science. 188, 109543.

693   Chávez-Andrade, G.M., Tanomaru-Filho, M., Basso Bernardi, M.I., de Toledo
694   Leonardo, R., Faria, G., Guerreiro-Tanomaru, J.M., 2019. Antimicrobial and
695   biofilm anti-adhesion activities of silver nanoparticles and farnesol against
696   endodontic microorganisms for possible application in root canal treatment.
697   Archives of Oral Biology. 107, 104481.

698   Dalsasso, R.R., Valencia, G.A., Monteiro, A.R., 2022. Impact of drying and extractions
699   processes on the recovery of gingerols and shogaols, the main bioactive
700   compounds of ginger. Food Research International. 154, 111043.

701   Deyab, M.A., Mohsen, Q., Bloise, E., Lazzoi, M.R., Mele, G., 2022. Experimental and
702   theoretical evaluations on Oleuropein as a natural origin corrosion inhibitor for
703   copper in acidic environment. Scientific Reports. 12 (1), 7579.

704   El-Refai, A.A., Ghoniem, G.A., El-Khateeb, A.Y., Hassaan, M.M., 2018. Eco-friendly
705   synthesis of metal nanoparticles using ginger and garlic extracts as biocompatible
706   novel antioxidant and antimicrobial agents. Journal of Nanostructure in Chemistry.
707   8 (1), 71-81.

708   Farmoudeh, A., Shokoohi, A., Ebrahimnejad, P., 2021. Preparation and evaluation of
709   the antibacterial effect of chitosan nanoparticles containing ginger extract tailored

by central composite design. Advanced Pharmaceutical Bulletin. 11 (4), 643-650.

Fazal, B.R., Becker, T., Kinsella, B., Lepkova, K., 2022. A review of plant extracts as green corrosion inhibitors for CO2 corrosion of carbon steel. npj Materials Degradation. 6 (1), 5.

Fouda, A.E.-A.S., Nazeer, A.A., Ibrahim, M., Fakih, M., 2013. Ginger extract as green corrosion inhibitor for steel in sulfide polluted salt water. Journal of the Korean Chemical Society. 57 (2), 272-278.

Garcia, M., Procopio, L., 2020. Distinct profiles in microbial diversity on carbon steel and different welds in simulated marine microcosm. Current Microbiology. 77 (6), 967-978.

Gurunathan, S., Han, J.W., Eppakayala, V., Jeyaraj, M., Kim, J.H., 2013. Cytotoxicity of biologically synthesized silver nanoparticles in MDA-MB-231 human breast cancer cells. BioMed Research International. 2013, 535796.

Hansen, D.S., Bram, M.V., Lauridsen, S.M.Ø., Yang, Z., 2021. Online quality measurements of total suspended solids for offshore reinjection: a review study. Energies. 14 (4), 967.

Hayat, S., Muzammil, S., Rasool, M.H., Nisar, Z., Hussain, S.Z., Sabri, A.N., Jamil, S., 2018. In vitro antibiofilm and anti-adhesion effects of magnesium oxide nanoparticles against antibiotic resistant bacteria. Microbiology and Immunology. 62 (4), 211-220.

Huh, A.J., Kwon, Y.J., 2011. "Nanoantibiotics": a new paradigm for treating infectious diseases using nanomaterials in the antibiotics resistant era. Journal of Controlled Release. 156 (2), 128-145.

Jain, S., Mehata, M.S., 2017. Medicinal plant leaf extract and pure flavonoid mediated green synthesis of silver nanoparticles and their enhanced antibacterial property. Scientific reports. 7 (1), 15867.

Jebril, S., Jenana, R.K.B., Dridi, C., 2020. Green synthesis of silver nanoparticles using Melia azedarach leaf extract and their antifungal activities: In vitro and in vivo. Materials Chemistry and Physics. 248, 122898.

Kaabipour, S., Hemmati, S., 2021. A review on the green and sustainable synthesis of silver nanoparticles and one-dimensional silver nanostructures. Beilstein Journal of Nanotechnology. 12, 102-136.

Kamli, M.R., Malik, M.A., Lone, S.A., Sabir, J.S.M., Mattar, E.H., Ahmad, A., 2021. Beta vulgaris assisted fabrication of novel Ag-Cu bimetallic nanoparticles for growth inhibition and virulence in Candida albicans. Pharmaceutics. 13 (11), 1957.

Karimi-Maleh, H., Mousavi, S.J., Mahdavian, M., Khaleghi, M., Bordbar, S., Yola, M.L., Darabi, R., Liu, M., 2021. Effects of silver nanoparticles added into polyurea coating on sulfate-reducing bacteria activity and electrochemical properties; an environmental nano-biotechnology investigation. Environmental Research. 198, 111251.

Khan, M., Hussain, M., Djavanroodi, F., 2021. Microbiologically influenced corrosion in oil and gas industries: A review. International Journal of Corrosion and Scale Inhibition. 10 (1), 80-106.

Lahiri, D., Nag, M., Sheikh, H.I., Sarkar, T., Edinur, H.A., Pati, S., Ray, R.R., 2021. Microbiologically-synthesized nanoparticles and their role in silencing the biofilm signaling cascade. Frontiers in Microbiology. 12, 636588.

Lee, E.-s., Hwang, H.-R., Kang, S.-M., Baekil Kim, 2019. Antibacterial effect of Zingiberaceae extracts mediated photodynamic therapy on Streptococcus mutans. The Journal of the Korean Dental Association. 57 (10), 560-568.

Li, H.N., Zhong, X.K., Hu, J.Y., Wang, J., Yu, J.S., 2022. The inhibition of sulfate

reducing bacteria adhesion and corrosion on the carbon steel surface using ZnO particles. Journal of Adhesion Science and Technology. Online, 1-14.

Liu, Y., Song, Z., Wang, W., Jiang, L., Zhang, Y., Guo, M., Song, F., Xu, N., 2019. Effect of ginger extract as green inhibitor on chloride-induced corrosion of carbon steel in simulated concrete pore solutions. Journal of Cleaner Production. 214, 298-307.

López-Ubaldo, F., Sánchez-Mendieta, V., Olea-Mejía, O.F., González-Pedroza María, S., Morales Luckie, R.A., 2020. Biosynthesis of Ag/Cu bimetallic nanoparticles using Ricinus communis and their antibacterial and antifungical activity. Advances in Natural Sciences: Nanoscience and Nanotechnology. 11 (2), 025018.

Loto, R.T., Loto, C.A., Akinyele, M., 2020. Effect of ginger, pomegranate and celery extracts on zinc electrodeposition, surface morphology and corrosion inhibition of mild steel. Alexandria Engineering Journal. 59 (2), 933-941.

Marslin, G., Siram, K., Maqbool, Q., Selvakesavan, R.K., Kruszka, D., Kachlicki, P., Franklin, G., 2018. Secondary metabolites in the green synthesis of metallic nanoparticles. Materials. 11 (6), 940.

Merugu, R., Gothalwal, R., Deshpande, P.K., De Mandal, S., Padala, G., Chitturi, K.L., 2021. Synthesis of Ag/Cu and Cu/Zn bimetallic nanoparticles using toddy palm: Investigations of their antitumor, antioxidant and antibacterial activities. Materials Today: Proceedings. 44, 99-105.

Moritz, M., Geszke-Moritz, M., 2013. The newest achievements in synthesis, immobilization and practical applications of antibacterial nanoparticles. Chemical Engineering Journal. 228, 596-613.

Narenkumar, J., Parthipan, P., Usha Raja Nanthini, A., Benelli, G., Murugan, K., Rajasekar, A., 2017. Ginger extract as green biocide to control microbial corrosion of mild steel. 3 Biotech. 7 (2), 133.

Nasser, B., Saito, Y., Alarawi, M., Al-Humam, A.A., Mineta, K., Gojobori, T., 2021. Characterization of microbiologically influenced corrosion by comprehensive metagenomic analysis of an inland oil field. Gene. 774, 145425.

Parmar, S., Kaur, H., Singh, J., Matharu, A.S., Ramakrishna, S., Bechelany, M., 2022. Recent advances in green synthesis of Ag NPs for extenuating antimicrobial resistance. Nanomaterials. 12 (7), 1115.

Patra, J.K., Das, G., Fraceto, L.F., Campos, E.V.R., Rodriguez-Torres, M.D.P., Acosta-Torres, L.S., Diaz-Torres, L.A., Grillo, R., Swamy, M.K., Sharma, S., Habtemariam, S., Shin, H.S., 2018. Nano based drug delivery systems: recent developments and future prospects. Journal of Nanobiotechnology. 16 (1), 1-33.

Pereira, G.F., Pilz-Junior, H.L., Corção, G., 2021. The impact of bacterial diversity on resistance to biocides in oilfields. Scientific Reports. 11 (1), 23027.

Procópio, L., 2022. Microbially induced corrosion impacts on the oil industry. Archives of Microbiology. 204 (2), 1-6.

Rabus, R., Boll, M., Heider, J., Meckenstock, R.U., Buckel, W., Einsle, O., Ermler, U., Golding, B.T., Gunsalus, R.P., Kroneck, P.M.H., Krueger, M., Lueders, T., Martins, B.M., Musat, F., Richnow, H.H., Schink, B., Seifert, J., Szaleniec, M., Treude, T., Ullmann, G.M., Vogt, C., von Bergen, M., Wilkes, H., 2016. Anaerobic microbial degradation of hydrocarbons: from enzymatic reactions to the environment. Journal of Molecular Microbiology and Biotechnology. 26 (1-3), 5-28.

Ramzan, M., Karobari, M.I., Heboyan, A., Mohamed, R.N., Mustafa, M., Basheer, S.N., Desai, V., Batool, S., Ahmed, N., Zeshan, B., 2022. Synthesis of silver nanoparticles from extracts of wild ginger (Zingiber zerumbet) with antibacterial activity against selective multidrug resistant oral bacteria. Molecules. 27 (6), 2007.

810 Saleh, R.M., Kabli, S.A., Al-Garni, S.M., Al-Ghamdi, M.A., Abdel-Aty, A.M.,
811   Mohamed, S.A., 2018. Solid-state fermentation by Trichoderma viride for
812   enhancing phenolic content, antioxidant and antimicrobial activities in ginger.
813   Letters in Applied Microbiology. 67 (2), 161-167.
814 Seetha, J., Mallavarapu, U.m., Akepogu, P., Mesa, A., Gollapudi, V.R., Natarajan, H.,
815   Anumakonda, V.R., 2020. Biosynthesis and study of bimetallic copper and silver
816   nanoparticles on cellulose cotton fabrics using Moringa oliefiera leaf extraction as
817   reductant. Inorganic and Nano-Metal Chemistry. 50 (9), 828-835.
818 Shaker, M.A., Shaaban, M.I., 2017. Synthesis of silver nanoparticles with antimicrobial
819   and anti-adherence activities against multidrug-resistant isolates from
820   Acinetobacter baumannii. Journal of Taibah University Medical Sciences. 12 (4),
821   291-297.
822 Subramanian, A.K., Arumugam, S., Mallaiya, K., Subramaniam, R., 2013. Synergistic
823   effect on corrosion inhibiton efficiency of ginger affinale extract in controlling
824   corrosion of mild steel in acid medium. Journal of the Korean Chemical Society.
825   57 (6), 672-676.
826 Sumbal, Nadeem, A., Naz, S., Ali, J.S., Mannan, A., Zia, M., 2019. Synthesis,
827   characterization and biological activities of monometallic and bimetallic
828   nanoparticles using Mirabilis jalapa leaf extract. Biotechnology Reports. 22,
829   e00338-e00338.
830 Tripathi, A.K., Saxena, P., Thakur, P., Rauniyar, S., Samanta, D., Gopalakrishnan, V.,
831   Singh, R.N., Sani, R.K., 2022. Transcriptomics and functional analysis of copper
832   stress response in the sulfate-reducing bacterium Desulfovibrio alaskensis G20.
833   International Journal of Molecular Sciences. 23 (3), 1396.
834 Yang, M., Shao, Z.-Y., Liao, X.-L., Xu, W.-F., Zhang, Y.-Y., 2020. Antibacterial activity
835   of Ag nanoclusters hydrogel to sulfate reducing bacteria in oil field pipeline.
836   Chinese Journal of Analytical Chemistry. 48 (12), 1674-1680.
837 Zhai, X., Li, K., Guan, F., Sun, C., Duan, J., Hou, B., 2018. Corrosion behavior of the
838   chitosan-zinc composite films in sulfate-reducing bacteria. Surface and Coatings
839   Technology. 344, 259-268.
840

Declaration of interests

☒ The authors declare that they have no known competing financial interests or personal relationships that could have appeared to influence the work reported in this paper.

☐The authors declare the following financial interests/personal relationships which may be considered as potential competing interests: